Molecular Crystals and Liquid Crystals

Publication details, including instructions for authors and subscription information:
http://www.tandfonline.com/loi/gmcl20

Light-Controlled Polymerization Kinetics for the Photostabilization of Cholesteric Fingerprint Rolls

Kyongok Kang [a] & Samuel Sprunt [a]

[a] Department of Physics, Kent State University, Kent, Ohio, USA

Version of record first published: 22 Sep 2010

To cite this article: Kyongok Kang & Samuel Sprunt (2007): Light-Controlled Polymerization Kinetics for the Photostabilization of Cholesteric Fingerprint Rolls, Molecular Crystals and Liquid Crystals, 466:1, 23-38

To link to this article: http://dx.doi.org/10.1080/15421400701246226

Mol. Cryst. Liq. Cryst., Vol. 466, pp. 23–38, 2007

ISSN: 1542-1406 print/1563-5287 online
DOI: 10.1080/15421400701246226

Taylor & Francis
Taylor & Francis Group

Light-Controlled Polymerization Kinetics for the Photostabilization of Cholesteric Fingerprint Rolls

Kyongok Kang
Samuel Sprunt
Department of Physics, Kent State University, Kent, Ohio, USA

We use a focused ultraviolet (UV) laser beam to photopolymerize localized polymer networks in a cholesteric liquid-crystalline host and to thereby stabilize small, light-diffracting "fingerprint" domains within a uniform, planar-aligned sample. As we have previously described, these "microspot" gratings are electrically switchable [1] and can be produced with diameters ranging from a few tens to hundreds of microns. Our focus in this article is to model the growth of the stabilized domain using a simple reaction-diffusion model of the photopolymerization process and to compare this model with data for networks formed both from isotropic and mesogenic monomers. In spite of an initial spatial asymmetry observed in the mesogenic case, both types of light-controlled networks develop in accordance with the fast photoreactivity/weak diffusion limit of the model.

Keywords: cholesteric "finger print" rolls; fast-reaction and weak-diffusion process; photopolymerization

1. INTRODUCTION

Electro-optic thin-film diffraction technology relies on the anchoring of liquid-crystalline molecules on a substrate, where light propagation characteristics depend on the molecular orientation at the interface. Cholesteric liquid crystals (CLC) can be used for various optical device applications of this kind, including electrically switchable responsive planar diffraction gratings, light modulators, and efficient electro-optic displays [2–7]. Especially the spatially periodic feature of the cholesteric "fingerprint" texture can be used directly to make diffraction gratings [8–10]. Typical switching times between the planar

Address correspondence to Kyongok Kang, Forschungszentrum Juelich, IFF Weiche Materie (soft matter), D 52425 Juelich, Germany. Tel: +49 2461-61-2149, Fax: +49 2461-61-2280. E-mail: k.kang@fz-juelich.de

diffracting (on) and homeotropic (off) states of CLCs are of the order of 10 ms using typical field strengths of the order of a few volts per micron [1,11,12]. The tailoring of electro-optic properties of such devices may be rather complicated. Liquid-crystalline material parameters such as helical pitch, dielectric anisotropy, and elastic and viscous damping characteristics are important, and in addition the types of added compounds—dyes and reactive monomers—affect the electro-optical properties of the grating. External driving factors such as the strength and direction of the applied electric field as well as the anchoring conditions at the surfaces of optical substrates determine the efficiency of these devices. Typical monodomains of the planar helical state can be achieved when the sample thickness is of the order of the liquid-crystalline pitch, giving rise to efficient planar diffraction gratings based on birefringence, confined between parallel, homogeneously aligning substrates. For a given wavelength, diffraction properties of gratings and planar dielectric waveguides can be formulated in terms of space harmonics propagating in anisotropic media [13] and planar dielectric waveguides [14,15] due to a well-defined regular spacing. Especially when the electric field of the incident light has a component perpendicular to the cholesteric twist axis and the wavelength of the phase fluctuation is comparable with its amplitude and the wavelength of light, the ratio of the wavelength of light to the periodicity of the grating is crucial to determine diffraction gratings as either a Raman–Nath or a Bragg type. However, cholesteric diffraction gratings can be produced in both Raman–Nath and Bragg regimes, depending on the ratio L/Λ of the thickness L and the periodicity Λ of the grating. Thus, both gratings can be uniquely oriented with the molecules with a field-induced response, depending on the cell thickness and cholesteric pitch [16]. Thus, polymer-stabilized cholesteric diffraction gratings (PSCDGs) are efficient, electrically controllable transmission gratings operating at low voltage of electric fields [1,11,12]. Their electro-optic performances, where both mesogenic and isotropic monomers in cholesterics are used under UV-curing conditions, are discussed in detail in Ref. 1. Independently there is also an interest in the propagation of light through inhomogeneous media, such as the localization and transport of electromagnetic energy in photonic devices, and modulational waveguides [17–20]. The transport of light through dielectrically inhomogeneous systems is also relevant for the production of gratings by means of photopolymerization. In the fabrication of such devices, propagation of light in combination with the relevant reaction-diffusion processes can play an important role. The spatial structures of CLCs can be embedded in a stabilizing polymer matrix via light-controlled polymerization

and are referred to as photopolymerized CLCs, an efficient confining template of the periodic molecules. The dynamics of the resulting distorted cholesteric liquid-crystalline structures, both for isotropic and mesogenic polymer networks, has been studied by dynamic light scattering in Ref. 21. Light-induced polymerization is a convenient means to stabilize spatially modulating structures of cholesteric fingerprint textures, where especially laser-controlled photostabilization in combination with an *in situ* external electric field is useful. Polymer networks of different architecture have been studied by UV irradiation of various monomer blends (such as radical and cationic types), with various types of photo initiators and under different UV-curing conditions [22]. The energy absorption in chemical reactions during polymerization is due to short-lived transients, such as radicals present during the UV-irradiation curing reaction [22,23]. The characteristic reactivity for photopolymerization can be used to make tunable photonic band gap materials using polymer-cholesteric liquid-crystalline composites and anisotropic gels [24,25]. To study the role of diffusion of radicals during polymerization, one can use real-time Fourier Transform Infrared (FTIR) spectroscopy and two-photon-induced photopolymerization in holographic recording [24]. In the present article, we employed a one-photon-induced optical tailoring in UV photopolymerization of a relatively well-ordered system of helicoidal structures whose pitch is of the order of optical wavelengths. This allows us to observe the light-controlled growth kinetics of photopolymerized cholesteric fingerprint rolls in space and time. We propose a simple model for the photopolymerization process in CLCs in the fast photo reactivity and weak diffusion limit under an optimum localized, focused UV-laser-beam illumination.

This article is organized as follows. In Section 2, a simple reaction-diffusion model is presented to describe the overall kinetics of the growth of photostabilized regions during UV curing. In Subsection 3.1, the materials and the experimental setup are introduced. Experimental results on growth kinetics and a quantitative comparison with the reaction-diffusion model are given in Subsection 3.2. Section 4 is a summary and discussion.

2. REACTION-DIFFUSION MODEL FOR THE COHERENT UV-INDUCED PHOTOPOLYMERIZATION PROCESS

Reaction-diffusion models describe the spatio-temporal evolution of patterns that are formed by the interplay between reaction kinetics and diffusive mass transport. The complexity of these models constitute a

challenge for the fundamental understanding of pattern formation kinetics at the molecular level, including the roles played by monomer functionality, diffusion of radicals, photo reactivity, and photo initiator absorption. In this section, we present a relatively simple reaction-diffusion model to describe the spatio-temporal development of cholesteric fingerprint rolls in the polymer network, depending on the UV laser intensity, exposure time, and fast photo reactivity. A Gaussian laser beam is used as a light source to control the kinetics of photopolymerization of the cholesteric fingerprint rolls that are formed by the *in situ* external electric field. We assume a radially symmetric evolution of the polymerized region as induced by the well-defined Gaussian laser beam. The reaction rate and diffusion constant for the monomers are assumed to be isotropic and depend on only the radial distance from the center of a Gaussian beam, which sets the center of symmetry for photostabilized regions [12]. In this case, the concentration of radicals is proportional to the laser light intensity, and this radical concentration is in turn proportional to the reaction rate, which may differ from the linear chain reactions. Then the dynamical equations for describing the photopolymerization process are [23,24]

$$\frac{\partial M(r,t)}{\partial t} = -F(r,t)I(r)M(r,t) + \frac{\partial}{\partial r}\left(D(r,t)\frac{\partial M(r,t)}{\partial r}\right) \tag{1}$$

$$\frac{\partial P(r,t)}{\partial t} = F(r,t)I(r)M(r,t), \tag{2}$$

where M is the concentration of monomer, P is the total concentration of polymerized monomers during the UV photocuring process, r is the radial distance from the center of the Gaussian beam, and t is the exposure time, that is, the time after which the UV laser has been switched on. The space- and time-dependent photoreactivity and diffusion coefficient of the monomers are written as $F(r,t) = F_0 \exp[-\kappa P(r,t)]$ and $D(r,t) = D_0 \exp[-\kappa P(r,t)]$, respectively, where the parameter κ controls the degree of inhibition of monomer reaction rates and diffusion due to the presence of already-formed photo-induced polymers: diffusion of monomers is hindered by the presence of polymers whereas monomers do not react with the monomers that already have been fully polymerized. Because the reaction rates are proportional to the laser light intensity $I(r)$ [26], the spatial variation of the Gaussian laser intensity is considered with a width equal to an aperture radius r_a, which fixes the spot size, and a half-waist width r_0 (the distance from the center where the intensity of the focal conic UV laser beam dropped by a factor of $1/e^2$),

$$I(r) = \begin{cases} I_0 \exp\left(-\frac{r^2}{r_0^2}\right) & (\mathrm{r<ra}) \\ 0 & (\mathrm{r > ra}) \end{cases}. \tag{3}$$

The boundary conditions for Eqs. (1) and (2) are $M(r, t = 0) = M_0$, $M(r, t = \infty) = 0$, and $P(r, t = 0) = 0$.

Let us consider two possible approximations, that is, feasible restrictions for the local inhibition of the photoreactivity $F(r, t)$ and diffusion coefficient $D(r, t)$: (1) a "mean-field" approach wherein the exponentials for $F(r, t)$ and $D(r, t)$, the polymerized amount of monomer $P(r, t)$, are replaced by the average value $\overline{P}$, which is the time- and spatial-averaged total concentration of polymerized monomers, and (2) the so-called reaction-depletion limit, where $F_0\, \mathrm{e}^{-\kappa \overline{P}}\, I_0 \equiv F_0' I_0 \gg D_0 r_0^{-2}$. The applicability may be estimated for low-concentration diacrylate polymerization in a liquid-crystalline host using $F_0' \simeq 4 \times 10^{-3} \mathrm{s}^{-1} \mathrm{mW}^{-1} \mathrm{cm}^2$ and $D_0 \simeq 10^{-7} \mathrm{cm}^2 \mathrm{s}^{-1}$. For the experimental conditions, with $I_0 \simeq 10\,\mathrm{mW cm}^{-2}$ and $r_0 \simeq 0.01\,\mathrm{cm}$, we then find $D/F_0' I_0 {r_0}^2 \simeq 0.03$. In this limit, Eqs. (1) and (2) may be simplified as

$$\frac{\partial M(r,t)}{\partial t} = -F_0' I_0 \exp\left(-\frac{r^2}{r_0^2}\right) M(r,t) = -\frac{\partial P(r,t)}{\partial t} \tag{4}$$

for $r < r_a$, with the additional boundary condition $P(r,t = \infty) = M_0$, with M_0 being the initial monomer concentration. The solutions to Eq. (4) that satisfy the boundary conditions are

$$M(r,t) = M_0 \exp\left[-F' I_0 \exp\left(-\frac{r^2}{r_0^2}\right) t\right] (r < r_a), \tag{5}$$

$$P(r,t) = M_0 \left\{1 - \exp\left[-F' I_0 \exp\left(-\frac{r^2}{r_0^2}\right) t\right]\right\} \quad (r < r_a) \tag{6}$$

as $M(r,t) = M_0$ and $P(r,t) = 0$ for $r > r_a$. The evolution of $P(r,t)/M_0$ is plotted in Fig. 1, where $\eta = F' I_0 t$ is the dimensionless time and $\xi = r/r_0$ the dimensionless distance from the center of the beam. Let us define a radius r_s corresponding to the size of the stabilized region of cholesteric fingerprint texture, as $\gamma M_0\, (0 < \gamma < 1)$. This defines a threshold concentration related to photo-induced polymerization. We may then calculate from Eq. (6) that

$$\left(\frac{r_s}{r_a}\right)^2 = \left(\frac{r_a}{r_0}\right)^2 \mathrm{In}\left[\frac{F' I_0}{\mathrm{In}(1-\gamma)^{-1}} t\right]. \tag{7}$$

The radius r_s is measured from the experimental photo-induced stabilized textures, and its maximum value is the radius of aperture r_a. This maximum occurs at the time of saturation

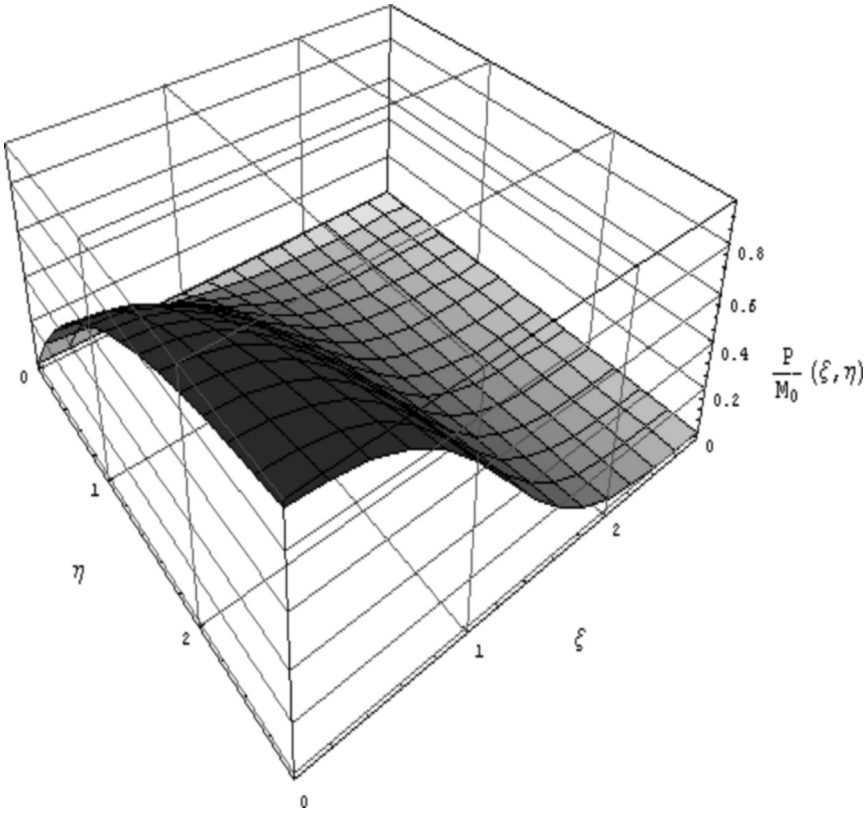

FIGURE 1 Simple evolutionary model of photopolymerization in choelsteric fingerprint rolls: reduced photopolymerization against monomer concentration, $P(\xi,\eta)/M_0$, as functions of dimensionless time ($\eta = F'I_0t$) and radius ($\eta = F'I_0t$).

$$t = t_1 = \exp\left(\frac{r_0^2}{r_a^2}\right)\frac{\ln(1-\gamma)^{-1}}{F'I_0}, \tag{8}$$

which follows from Eq. (7). Note that at time $t < t_0 = \frac{\ln(1-\gamma)^{-1}}{F'I_0}$, where $r_s = 0$, no stabilized domain is formed yet, that is, t_0 is a threshold time before which no stabilization is achieved. We thus find the following time dependence of the size of the polymer-stabilized region, within the reaction-depletion limit,

$$\left(\frac{r_s}{r_a}\right)^2 = \begin{cases} 0 & (t < t_0) \\ \left(\frac{r_a}{r_0}\right)^2 \ln\left(\frac{t}{t_0}\right) & (t_0 < t < t_1). \\ 1 & (t > t_1) \end{cases} \tag{9}$$

Domain sizes grow logarithmically in time, whereas the ratio determines how fast UV absorbed energy is involved to polymerize monomers between the threshold time t_0 and the saturation time t_1, as defined earlier.

We also compare our experiments with a weak diffusion perturbation theory, where Eqs. (1) and (2) are solved by iteration to calculate the leading order correction to Eq. (5), due to a perturbation contribution of fast photoreactivity compared to weak diffusion. One can write the monomer concentration as $M = M^{(0)} + M^{(1)}$, where $M^{(0)}$ is given by Eq. (5) and $M^{(1)}$ is the small perturbation of the monomer concentration resulting from the first correction due to the finite monomer diffusivity. Similarly, we can write the photo-induced polymerization as $P = P^{(0)} + P^{(1)}$, where $P^{(0)}$ is given by Eq. (6). Substituting into Eqs. (1) and (2) and again introducing the dimensionless distance $\xi \equiv r/r_0$ and (photo reactive) time $\eta \equiv F' I_0 t$ leads to

$$\frac{\partial M^{(1)}}{\partial \eta} = -\exp\left(-\xi^2\right) M^{(1)} + \varepsilon \frac{\partial^2 M^{(0)}}{\partial \xi^2}, \tag{10}$$

$$\frac{\partial P^{(1)}}{\partial \eta} = \exp\left(-\xi^2\right) M^{(1)}, \tag{11}$$

the first order in the small perturbative quantities $\varepsilon \equiv D_0/F' I_0 r_0^2$, $M^{(1)}$, and $P^{(1)}$. By inserting Eqs. (5) and (6) into Eqs. (10) and (11) and solving the resulting first-order differential equation, we obtain

$$\begin{aligned} \frac{P(\xi,\eta)}{M_0} = \frac{P^{(0)}(\xi,\eta) + P^{(1)}(\xi,\eta)}{M_0} &= \left[1 + 2\varepsilon(2\xi^2 + 1)\exp\left(\xi^2\right)\right] \\ &\times \left\{1 - \exp\left[-\exp\left(-\xi^2\right)\eta\right]\right\} + \varepsilon\eta \exp\left[-\exp\left(-\xi^2\right)\eta\right] \\ &\times \left\{2(2\xi^2 + 1) + (2\xi^2 + 1)\exp\left(-\xi^2\right)\eta + \frac{4}{3}\xi^2\eta^2 \exp\left(-2\xi^2\right)\right\}. \end{aligned} \tag{12}$$

This result is plotted in Fig. 2 for various values of ε from 0 up to 0.2. The main effect of weak diffusion is clearly to draw more monomer into the central region of exposure, where the rate of monomer depletion is highest, and thereby produce a local polymer concentration higher than M_0. The impact on r_s is negligible, except for the longest time (largest η).

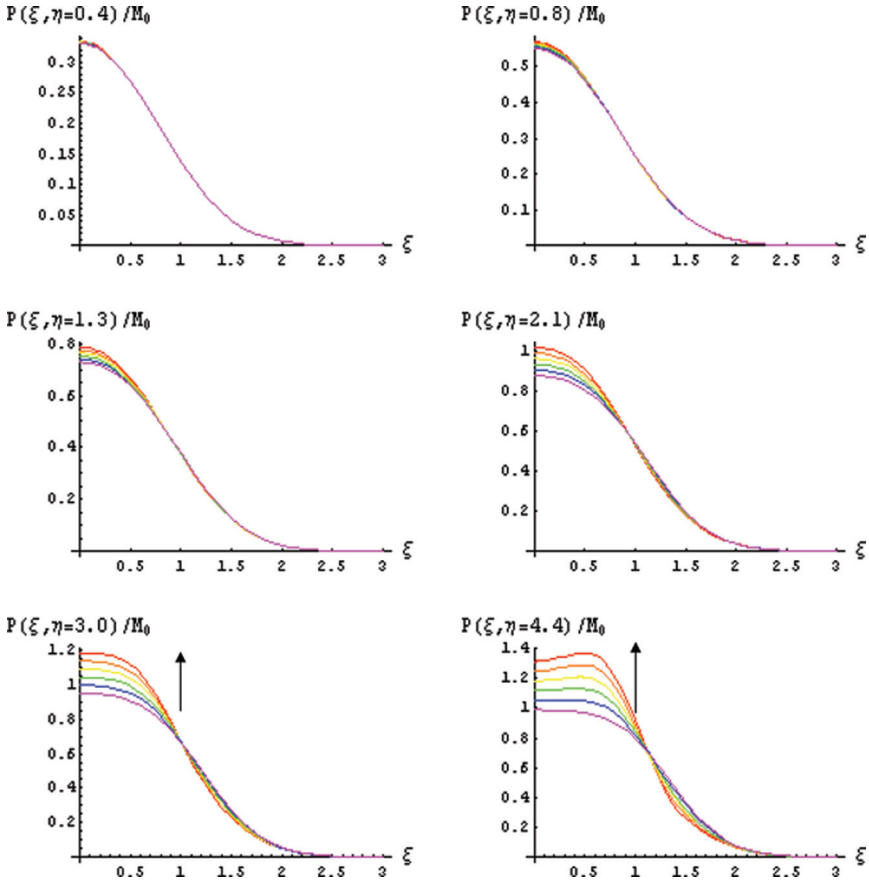

FIGURE 2 Calculation of weak diffusion limit of photopolymerization with perturbation theory: photoreactivity compared to diffusive behavior is chosen as a perturbative parameter $(\varepsilon \equiv D_0/F'I_0r_0^2)$. The photopolymerization against monomer concentration is increasing in spatial–temporal phase $(\eta = F'I_0t,\ \xi \equiv r/r_0)$ from $\varepsilon = 0,\ \varepsilon = 0.04,\ \varepsilon = 0.08, \varepsilon = 0.12,\ \varepsilon = 0.16,$ to $\varepsilon = 0.20$ as from below to the top line in each graph, shown in arrows.

3. EXPERIMENTS

In this section, we introduce the details of the experimental materials and setup, present experimental results on growth kinetics together with a comparison to the reaction-diffusion model, and finally describe the optical morphology of light-controlled photostabilized cholesteric fingerprint rolls in space and time.

3.1. Experimental Details: Materials and the UV-Laser-Focused Microspot in situ Polymerization Setup

The initial sample mixture contains 96.6% cholesteric liquid crystal (Merck E44 with 0.4% chiral dopant R-1011), 3% photoreactive monomer, and 0.15% photoinitiator (Irgacure 651 from CIBA-GEIGY). Two different low-molecular-weight monomer types are used—isotropic Hexanedioldiacrylate (HDDA) and mesogenic RM257—in the same cholesteric host. The photoinitiator (Irg651) reacts efficiently at 365 nm and represents a good compromise with the substrate transmission in our experiments, which is $\sim$52% at 365 nm. Compared to the earlier work related to PSCDGs, here we fix the optical pitch in our experiments at 10 μm, corresponding to 0.4 wt% of chiral dopant concentration [11] and an ITO-cell thickness comparable to the cholesteric pitch. Structure and morphology of PSCDGs have been studied with different UV incident polarizations, where, however, the UV incident beam was not coherent [12]. Here we employ a coherent UV-laser-focused (microspot) in situ photopolymerization [1], which enables the control of the growth of photopolymerized cholesteric fingerprint rolls. A schematic of the optical setup of UV laser microspot (or focused) in situ polymerization is shown in Fig. 3. A one-dimensional light-diffracting state is formed through nucleation and growth of helical domains of cholesteric rolls in the presence of an external electric field. The helicoidal axis of the

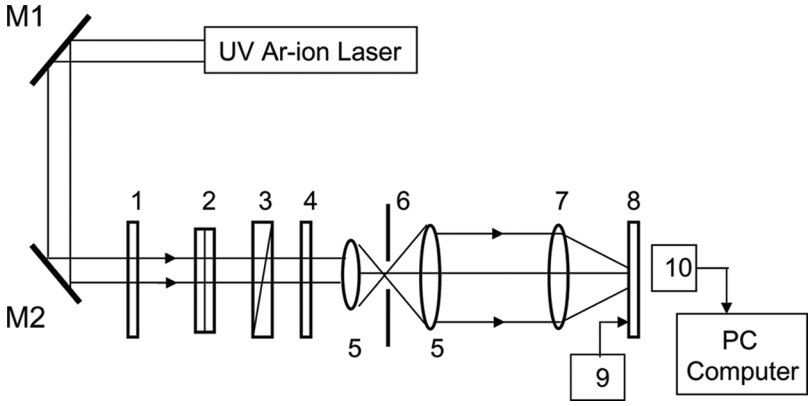

FIGURE 3 Optical setup of UV-focused microspot in situ photopolymerized cholesteric diffraction gratings: M1 and M2: mirrors, 1: bandpass filter (365 nm), 2: double neutral density filter, 3: polarizer, 4: half-wave plate, 5 and 6: spatial filters, 7: UV achromatic lens ($f = 75$ mm), 8: sample mount on X-Y stage, 9: function generator-amplifier, and 10: power detector.

cholesteric director is reoriented (or deformed) into the plane of the substrate (fingerprint rolls or planar state) and tuned by an electric field ($\sim$0.3–0.4 V/μm) from the initial state to the final state where the helix is relaxed to equilibrium with the substrate (normal state). A planar diffractive state is prepared before UV laser photopolymerization. The sample mixture is filled into an optically transparent ITO cell (EHC Co. Japan), which is exposed to a $\sim$1-kHz DC electric field. Then the internal polymer network can be fixed (or freezed) by the optically localized *in situ* setup (shown in Figs. 3 and 4a), with a focused Gaussian UV laser beam in TEM00 mode using an argon-ion laser (Lexel model 95), operating at 365 nm, whose beam diameter is focused such that the half-waist spot radius (where the intensity dropped by a factor of $1/e^2$; see Eq. (3) in Section 2.1) is approximately 100–400 μm. The polarization of the beam is linearly aligned along the helicoidal axis. The typical UV-laser power incident on the sample ranges from 0.1 to 25 mW, and the exposure times are 3 to 250 s. Photopolymerization can be done with multiple microspots in a sample, mounted on the micron-scaled x-y translational stage, as shown in Fig. 3. Also the spot size of a Gaussian beam can be varied through a change of the position of the sample mount. A UV achromatic lens ($f\sim$75 mm) is used to correct for chromatic aberration in the focal-conic zone. Thus we are able to control not only the location but also the size of photopolymerized cholesteric diffractive micrograting of the planar diffracting state (i.e., cholesteric fingerprint rolls). The quantitative measurement of the mean spot radius of photo-induced stabilized domains of cholesteric fingerprint rolls is done by individual microspot photopolymerization for a certain time span with a fixed UV laser power and with the *in situ* electric field. After UV photopolymerization for a certain time, the external electric field is turned off. Nonstabilized rolls will then disappear, and the average radius of photostabilized CLC fingerprint rolls are measured by means of depolarized microscopy. In this way, we probe the morphology of photopolymerized CLCs, where the UV exposure time and UV laser power are varied independently. We also monitored the size of the polymerized region by ceasing to UV-illuminate the sample. The optimal UV-curing conditions correspond to those parameters for which the maximum area is photostabilized. These optimum values of the previously mentioned variables for photopolymerization could be determined by monitoring the exposed area with time starting immediately after the beam was shut off. UV-curing conditions are independently determined with a focused spot size of polymer-stabilized CLC as a function of both the laser power, using a reduction filter, and the focal length of the achromatic lens. We have found the optimum UV condition for isotropic HDDA- and mesogenic

RM-networks in cholesterics to be around $2.5\,\mathrm{mW/cm^{-2}}$ and $10\,\mathrm{mW/cm^{-2}}$, respectively.

3.2. Growth Kinetics of the Photo-Induced Polymer-Stabilized Cholesteric Fingerprint Rolls

In the initial stages of growth, the photostabilized region is not exactly spherical but somewhat ellipsoidal. The size of the spot is then taken as equal to the average of the extension of the spot along the major and minor axis of the spot. The spatial distribution of photopolymerized cholesteric polymer networks is measured in time as a function of UV laser power at different exposure times. The optical morphology during the early stage of pattern formation (or cholesteric fingerprint rolls) is shown in Fig. 4b for several UV exposure times with a constant UV laser power in the presence of the external electric field. It shows the growth of photostabilized cholesteric fingerprint rolls within a slightly nonspherical overall region. At longer times, the overall shape of the texture coincides with the illuminated area of the Gaussian (TEM00-mode) UV laser field. The pronounced difference in optical appearance of the photopolymerized region and nonpolymerized region allows the determination of the sizes of the polymerized region and comparison it to the theoretical predictions in Section 2.1. The size of the interfacial domain between the photostabilized planar diffracting state and the surrounding normal state after cessation of the optical field is systematically measured as a function of the UV-exposure conditions. We assume that the fast photoreaction terminates rapidly after cessation of coherent UV illumination with a fixed focal-conic spot size. The size of the overall photostabilized domains with a cholesteric texture is plotted in Fig. 5 as a function of the UV-exposure time for the isotropic and mesogenic monomer type. The saturated diameter of the photopolymerized cholesteric domain is 300 and 270 μm for isotropic (HDDA) and mesogenic (RM257) monomer, respectively [1]. The normalized size of domains of photopolymerized cholesteric texture increases logarithmically in time and in accordance with the prediction from our reaction-diffusion model in Section 2. The size of domain in Fig. 5 has been scaled to the saturation radius r_a, and the time is scaled such that the threshold time t_0 and the saturation time t_1 correspond to 0 and 1, respectively. The solid line in Fig. 5 is a fit of the experimental data to a straight line for both RM257 and HDDA. Although both isotropic and reactive mesogenic monomer types of polymer network respond at different UV strengths (and also show different morphologies as can be seen from Fig. 6), their growth kinetics show the same behavior in terms of the

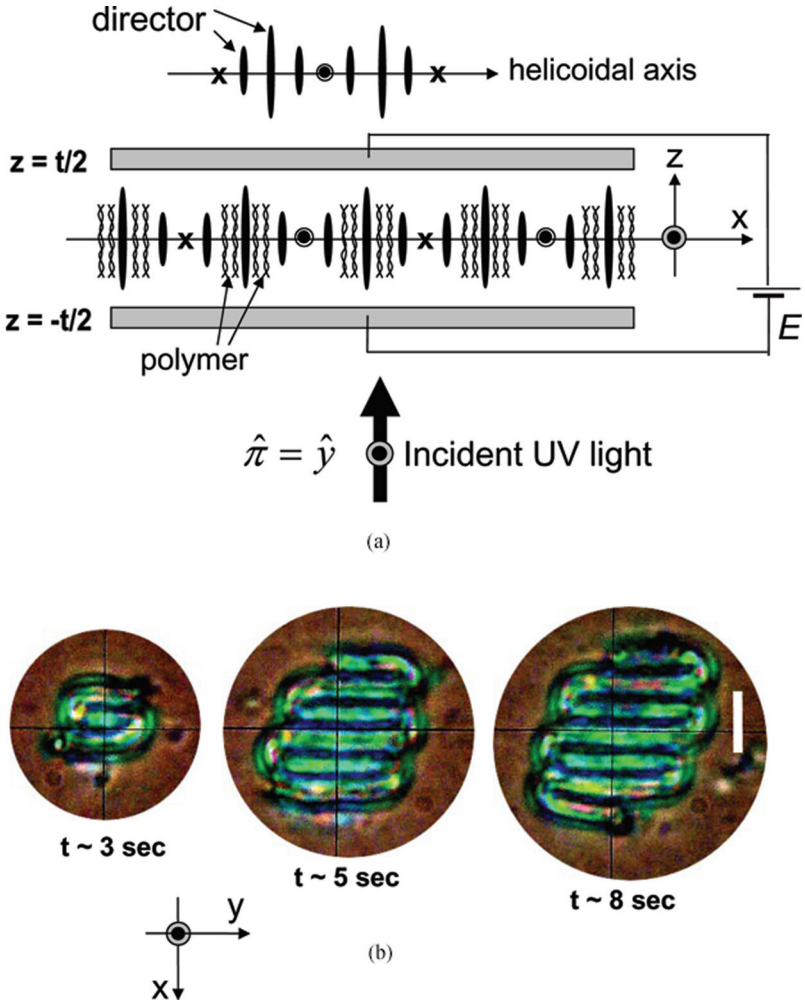

FIGURE 4 (a) Scheme drawing of a cholesteric diffraction grating with an incident UV light in z-direction with a polarization $\hat{\pi} = \hat{y}$ the overall director direction is indicated along the helicodal axis. (b) The evolutionary growth of photopolymerized cholesteric fingerprint rolls in the early stage of UV-curing polymerization (at different short exposure times and UV laser power $\sim 0.2\,\text{mW}$) in the presence of an electric field. The scale bar corresponds to $10\,\mu\text{m}$.

rescaled variables introduced previously, again in accordance with the reaction-diffusion model. The optical morphologies of isotropic and mesogenic types of networks in CLC are shown in Fig. 6 depending

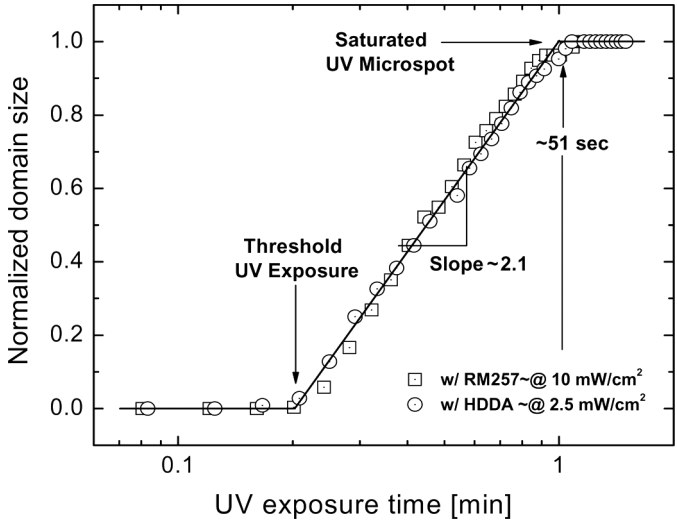

FIGURE 5 Growth of photopolymerized cholesteric domains in the microspot photo-induced Gaussian UV-curing setup; there are different kinetic times of photostabilization, (i.e., threshold UV exposure time, and the saturated time and logarithmically linear with a slope in time between them). The slope is compared our measurements for both isotropic and reactive-mesogenic monomers with a simple model as suggested in Section 4.1.

on lower/higher UV energy inside the focal-conic Gaussian UV illumination at a saturated domain. We have found a difference in the threshold UV energy of photostabilization in the CLC-polymer networks depending on the monomer type. The optimum UV laser intensity for HDDA is about four times smaller as compared to RM257, which suggests that roughly four times more UV energy for the mesogenic monomer type is needed to establish photostabilization as compared to the isotropic type of monomer. The threshold UV exposure time t_0 at which polymerization sets in, and the saturation UV time t_1 where photostabilization occurred to a maximum extent, can be quite accurately determined from the experimental data. According to the reaction-diffusion model discussed in Section 2, t_0 and t_1 differ for both monomer types because both κ and $\overline{P}$ will likely be different, for example because of the difference in the polymer network morphology. To reach the threshold exposure time, the reactive mesogenic type of monomer RM 257 needs more UV laser power than the isotropic type of monomer HDDA. The reason for this is probably that the mesogenic type of polymer network is more densely packed,

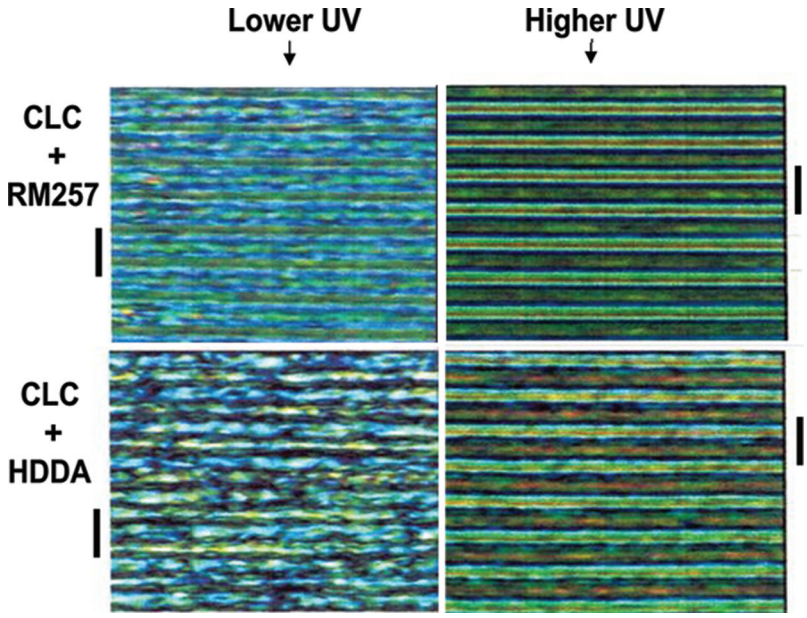

FIGURE 6 Optical morphologies of low and high UV energy in cholesterics; upper raw shows the reactive mesogenic RM 257 polymer network, and lower raw is for isotropic HDDA polymer network in cholesterics. The optical pitch is a bar of 10 μm for the morphology in the diffraction grating axis.

with a robust periodic structure (seen in the optical morphologies in Fig. 6). The inhibition effect for the development of a RM257 network is therefore likely to be significantly greater than for HDDA (i.e., the factor $e-\kappa^{\overline{P}}$ is likely significantly smaller). The slope of 2.1 of the fitted straight line in Fig. 5 should, according to Eq. (9), be equal to $(r_a/r_0)^2$. The slope of 2.1 is indeed equal to the value of $(r_a/r_0)^2$ as determined from the geometrical parameters of our experimental setup. Thus, within the optimum focused UV-curing condition, photostabilized CLCs are formed through a relatively slow diffusion process of monomers as compared to the reaction polymerization kinetics. In addition, we conclude that the size of the region where polymerization occurred to an extent that the liquid-crystalline structure is stabilized increases logarithmically in time, at least under optimum UV intensities. The first-order deviations from the weak diffusion limit as discussed at the end of Section 2.1 are apparently very small for the systems investigated in the present article but might be more relevant to other types of systems.

4. SUMMARY AND CONCLUSIONS

The light-controlled growth kinetics of polymerized cholesteric fingerprint rolls is described by means of a relatively simple reaction-diffusion model within the weak diffusion limit. Assuming a Gaussian UV-beam profile, this model predicts a logarithmic growth in time of the radius of photostabilized regions. In the very early stages of photostabilization, after a threshold UV exposure time, the photostabilized regions are somewhat ellipsoidal in shape but soon become spherical because of the light-controlled Gaussian beam photostabilization. Aside from this initial asymmetry of the photostabilized regions, the experimental growth kinetics is found to be in perfect agreement with the reaction-diffusion model: there is logarithmic growth until the photostabilized region is as large as the illuminated region, with a prefactor that is in accordance with the geometrical parameters of the experimental setup. The model applies to both the isotropic and mesogenic monomer type of networks. The light-controlled growth kinetics of both polymer networks in cholesterics is determined by fast photo reactivity and weak diffusivity. Also the photo-induced polymer-stabilized cholesteric fingerprint rolls are formed independent of the polarization direction of the UV laser beam.

The anchoring of CLCs is affected by the presence of the polymer matrix and is influenced by the spatial modulation of the periodic dielectric medium formed by the cholesteric polymer network. By tuning the focused UV energy, we have found diffractive planar propagation in the direction perpendicular to the fingerprint rolls (i.e., the direction along the helicoidal axis) independent of the incident light polarization. Although it is not clear how the UV light interacts with the modulated dielectric material, it would be an interesting subject for tailoring of electro-optical properties of a periodic dielectric medium. It remains a challenge to predict the formation of such periodic structures based on a theory for light propagation in optically anisotropic media such as periodically modulated dielectrics. Furthermore, the surface-relief and refractive-index-modulation profiles in highly diffractive devices can be used in phase relief/lock microelectro-optic channeling technology [27] and planar optic communications in nano-electronics as an integrated transport package.

ACKNOWLEDGMENTS

This research was supported by the Office of Naval Research under Grant No. N00014-99-1-0899 and by Advanced Liquid Crystal Optical

Materials/National Science Foundation (ALCOM/NSF) under Grant No. DMR-8920147.

REFERENCES

[1] Kang, K., Chien, L. C., & Sprunt, S. (2002). *Liquid Crystals*, *29*, 9–18.
[2] Subacius, D., Shiyanovskii, S. V., Bos, P., & Lavrentovich, O. D. (1997). *Appl. Phys. Lett*, *71*, 3323–3325.
[3] Schadt, M. & Helfrich, W. (1971). *Appl. Phys. Lett.*, *18*, 127.
[4] Wu, C. S. & Wu, S. T. (1992). *Proc. SPIE*, *1665*, 250.
[5] Crandall, K. A., Fisch, M. R., Petschek, R. G., & Rosenblatt, C. (1994). *Appl. Phys. Lett.*, *64*, 1741.
[6] Yang, D. K. & Doane, J. W. (1992). *SID International Symposium*, 759.
[7] Chilaya, G., Hauck, G., Koswig, H. D., & Sikharulidze, D. (1996). *J. Appl. Phys.*, *80*, 1907–1909.
[8] Sackmann, E., Meiboom, S., Snyder, C. L., Meixner, A. E., & Dietz, R. E. (1968). *J. Am. Chem. Soc.*, *90*, 3567.
[9] Kawachi, M., Kato, K., & Kogure, O. (1978). *Jpn. J. Appl. Phys.*, *17*, 1245.
[10] Suresh, K. A., Sunil Kumar, P. B., & Ranganath, G. S. (1992). *Liquid Crystals*, *11*(1), 73–82.
[11] Lee, S. N., Chien, L. C., & Sprunt, S. (1998). *Appl. Phys. Lett.*, *72*, 885.
[12] Kang, S. W., Sprunt, S., & Chien, L. C. (2000). *Appl. Phys. Lett.*, *76*, 3516–3518.
[13] Rokushima, K. & Yamakita, J. (1983). *J. Opt. Soc. Am.*, *73*(7), 901–908.
[14] Delavaux, J.-M. P., Chang, W. S. C., & Moharam, M. G. (1985). *Appl. Opt.*, *24*(2), 221–226.
[15] Davisson, C. & Germer, L. H. (1927). *Phys. Rev.*, *30*(6), 705–740.
[16] Stich, N. & Kitzerow, H. -S. (2005). *J. Appl. Phys.*, *97*, 033519.
[17] Pollack, S. E. (2002). *An Introduction to Acousto-Optics Fundamentals of Optics and Laser*, Univ. of Colorado: Boulder, CO; Physics 7810, http://faculty.washington.edu/skotep/pdfs/acoustooptics.pdf.
[18] Maier, S. A., Kik, P. G., Atwater, H. A., Meltzer, S., Harel, E., Koel, B. E., & Requicha, A. A. G. (2003). *Nature Materials*, *2*, 229–232.
[19] van der Wiel, W. G., De Franceschi, S., Elzermann, J. M., Fujisawa, T., Tarucha, S., & Kouwenhoven, L. P. (2003). *Rev. Mod. Phys.*, *75*, 1–22; de Lima, M. M., Alsina, F., Seidel, W., & Santos, P. V. (2003). *Jrnl. of Appl. Phys.*, *94*, 7848.
[20] Grzybowski, B. A., Bishop, K. J. M., Campbell, C. J., Fialkowski, M., & Smoukov, S. K. (2005). *Soft Matter*, *1*, 114–128.
[21] Kang, K. & Sprunt, S. (2005). *Phys. Rev. E.*, *72*, 031702.
[22] Decker, C. (2002). Light-induced cross-linking polymerization. *Polymer International*, *51*(11), 1141–1150.
[23] Scherzer, T. & Decker, U. (1999). Real-time FTIR-ATR spectroscopy to study the kinetics of ultrafast reactions induced by monochromatic UV light. *Vibr. Spectrosc.*, *19*, 385–398.
[24] Scherzer, T. (2002). Real-Time FTIR-ATR spectroscopy of photopolymerization reactions. *Macromol. Symp.*, *184*, 79–97.
[25] Kirkpatrick, S. M., Baur, J. W., Clark, C. M. Denny, L. R., Tomlin, D. W., Reinhard, B. R., Kannan, R., & Stone, M. O. (1999). *Appl. Phys. A.*, *69*, 461–464.
[26] Decker, C. & Jenkins, A. D. (1985). *Macromolecules*, *18*, 1241–1244.
[27] Herzig, H. P. (Ed). (1997). *Micro-optics: Elements, Systems, and Applications*, Taylor & Francis Ltd.: London